Experimentally-Benchmarked kinetic simulations of heat transfer through rarefied gas with constant heat flux at the boundary

M. Adnan Khan, Yann Jobic, Irina Martin Graur, Mustafa Hadj-Nacer, Cody Zampella, Miles Greiner

Version of Record: https://www.sciencedirect.com/science/article/pii/S0017931021004816
Manuscript_4ab278b8f2743ff42b4c1fe924baa412

Experimentally-Benchmarked Kinetic Simulations of Heat Transfer Through Rarefied Gas with Constant Heat Flux at the Boundary

M. Adnan Khan, Yann Jobic, Irina Graur,
Aix-Marseille Université, CNRS, IUSTI UMR 7343, 13013 Marseille, France,
Mustafa Hadj Nacer, Cody Zampella, Miles Greiner
Department of Mechanical Engineering, University of Nevada, Reno, NV, USA

Abstract

In many applications, the heat flux at the surface is known instead of the surface temperature. In addition, in some applications, like vacuum drying or high altitude flights, the pressure is below atmospheric pressure, so the rarefaction effects become important, and therefore, the Navier-Stokes-Fourier equations fail to predict gas thermal behavior. In this paper, a constant heat flux boundary condition is developed and implemented in the frame of the Shakhov model kinetic equation, with the possibility to simulate the diffuse-specular reflexion of the molecules from the surface. The developed technique is implemented for the simulation of gas heat transfer in a two concentric cylinders configuration, similar to vacuum drying of used nuclear fuel canisters. The numerical results obtained using developed approach are compared with experimental data of heat transfer through rarefied gas between two concentric cylinders.

1. Introduction

Thermal management is important in many application and may take place under low-pressure conditions, such as in vacuum drying, re-entry flights and development of thermal protection systems. In other applications, such as electronics as well as MEMS/NEMS systems, where the characteristic scale of the devices is small, thermal management is also important. Often, for these types of systems, a constant heat flux needs to be maintained at the boundary. In both type of applications, the Knudsen number (*i.e.* the ratio between the molecular mean free path and the characteristic flow dimension) is usually larger then 0.1. Under such conditions, specific effects, such as temperature jump or velocity slip, appear at the interface between gas and solid surface. In practice, often, the surface temperature is unknown, and only the heat flux through the interface can be measured or estimated. To obtain the information about the surface temperature, the constant heat flux boundary condition has to be developed. This type of condition is largely applied in case of continuum flow described in

the frame of the Navier-Stokes-Fourier model. However, when the gas becomes rarefied, the kinetic models need to be applied. Several applications of the constant heat flux boundary conditions in the frame of the Direct Simulation Monte Carlo (DSMC) method were discussed in Refs. [1, 2]. However, up to now, we found only one paper where a constant heat flux boundary condition, namely the constant zero heat flux at the solid surface, *i.e.* adiabatic condition, is implemented for the kinetic equation, which was numerically solved using the Discrete Velocity Method [3].

In this paper, we apply the constant heat flux boundary condition in the frame of the Shakhov model (S-model) kinetic equation [4] for two infinite concentric cylinders geometry. We do not restrict our study to the zero heat flux condition. In addition, the diffuse-specular reflexion of the molecules from the solid surface is implemented to better describe the gas-solid surface interaction. First, some general behaviors of the temperature and heat flux between the two concentric cylinders as a function of pressure are obtained under constant heat flux condition at the inner cylinder surface. Second, a comparison with the analytical solution of the Fourier equation is conducted in the continuum and slip regimes. Finally, the developed approaches are employed to simulate heat transfer in an experimental configuration, consisting of two concentric cylinders, and the results are compared with the experimental data.

2. Problem Formulation

In this paper, conduction heat transfer between two concentric cylinders separated by a rarefied gas at rest is considered, see Fig. 1. The radii of the inner and outer cylinders are R'_1 and R'_2, respectively. The temperature of the outer cylinder wall, $T'_{\rm w2}$, is known and maintained constant. Both cylinders are assumed to have an infinite length, so this heat transfer problem can be considered as one dimensional. Therefore, the heat flux has only one component in the direction normal to the surfaces, $\mathbf{q}' = (q'_r, 0, 0)$, which is denoted in following as q', by omitting r subscript. A constant heat flux, q'_1, is imposed at the inner cylinder.

The flow between the two cylinders is determined by the following parameters, the aspect ratio between the cylinders' radii, $\mathcal{R} = R'_1/R'_2$, the temperature of the outer cylinder surface, $T'_{\rm w2}$, and the heat flux on the inner cylinder surface, q'_1. The gas rarefaction is characterized by the rarefaction parameter, δ, defined as

$$\delta = \frac{R_0}{\ell}, \quad \text{where} \quad \ell = \frac{\mu_0 \upsilon_0}{p_0}, \quad \upsilon_0 = \sqrt{\frac{2k_{\rm B}T_0}{m}}. \tag{1}$$

In this expressions, R_0 is the reference space dimension, ℓ is the equivalent molecular free path at reference pressure p_0, υ_0 is the most probable molecular velocity at reference temperature, T_0, μ_0 is the gas viscosity calculated at the reference temperature: $\mu_0 = \mu(T_0)$, m is the molecular mass of the gas, and $k_{\rm B}$ is the Boltzmann constant. It is convenient to take the distance between the cylinders as the reference space dimension, $R_0 = R'_2 - R'_1$. The temperature of

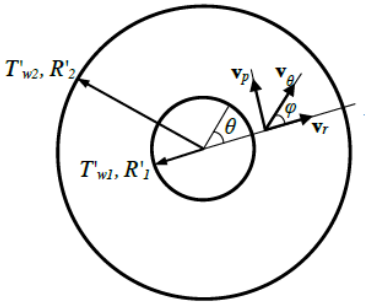

Figure 1: Cross-section of two concentric cylinders configuration: dimensions (r, θ) in physical space, dimensions $(\upsilon_r, \upsilon_\theta)$ (or (υ_p, φ)) in molecular velocity space.

the outer cylinder is used as the reference temperature, $T_0 = T'_{w_2}$. It should be noted that the rarefaction parameter is inversely proportional to the commonly used Knudsen number, $\delta \sim 1/Kn$.

The influence of the gas-surface interaction is taken into account by the thermal accommodation coefficient, denoted as

$$\alpha = \frac{T_i - T_r}{T_i - T_w}, \tag{2}$$

where T_i and T_r are the temperature of the incident and reflected molecules, respectively, and T_w is the wall temperature.

3. Continuum and Slip Flow Regimes

In the slip and continuum (hydrodynamic) flow regimes, the steady-state temperature distribution between two concentric cylinders is obtained from the energy balance

$$\frac{\partial}{\partial r'}\left(r'\kappa'\frac{\partial T'}{\partial r'}\right) = 0, \tag{3}$$

where r' is the radial coordinate of the annular region between the cylinders and κ' is the gas thermal conductivity. It is to note that the hypothesis of zero flow velocity is used, and only conduction heat transfer is considered. The Fourier law can be applied to calculate the radial heat flux as

$$q' = -\kappa'\frac{dT'}{dr'}. \tag{4}$$

For monoatomic gases, the gas thermal conductivity is related to the gas viscosity as follows

$$\kappa' = \frac{15}{4}\frac{k_{\mathrm{B}}}{m}\mu'. \tag{5}$$

The power-law temperature dependency of the viscosity coefficient is used [5] and is defined as

$$\mu' = \mu_0 \left(\frac{T'}{T_0} \right)^{\omega}, \tag{6}$$

where ω is the viscosity index, which is equal to 0.5 for the Hard Sphere model and 1 for the Maxwell model.

In the continuum flow regime, the temperature continuity condition may be assumed on the cylinders' walls. However, in the slip flow regime, the temperature jump [6] must be used as boundary condition at the gas-surface interface for Eq. (3)

$$T'_{\rm g} = T'_{\rm w} + \xi_{\rm T} \ell \frac{dT'}{dr'}\Big|_w, \tag{7}$$

where $T'_{\rm g}$ is the gas temperature near the wall, $T'_{\rm w}$ is the wall temperature, and $\xi_{\rm T}$ is the temperature jump coefficient [7], which depends on the gas nature and surface state through the thermal accommodation coefficient, α. The authors of Ref. [8] proposed the following expression for polyatomic gases,

$$\xi_T = \left(\frac{2-\alpha}{\alpha} + 0.17 \right) \frac{\sqrt{\pi}}{Pr} \frac{\gamma}{\gamma+1}, \tag{8}$$

which was obtained by applying a variational method to the Morse equation [9] and to the Holway model [10]. In Eq. (8), γ is the gas specific heat ratio and Pr is the Prandtl number. For monatomic gases, this expression is reduced to the one proposed by Welander [11]. For the case of complete accommodation ($\alpha = 1$) and a monatomic gas (γ=5/3 and Pr=2/3), the value of the temperature jump coefficient is $\xi_{\rm T} \sim 1.94$.

It is convenient to introduce the dimensionless variables as follows

$$r = \frac{r'}{R_0}, \qquad t = \frac{t'}{t_0}, \qquad T = \frac{T'}{T_0}, \qquad p = \frac{p'}{p_0}, \qquad q = \frac{q'}{p_0 \upsilon_0}, \qquad \mu = \frac{\mu'}{\mu_0}, \tag{9}$$

completed by the equation of state $p' = n' k_{\rm B} T'$. The dimensionless form of the temperature jump boundary conditions on the cylinders' walls becomes

$$T_g = \begin{cases} T_{\rm w1} + \frac{\xi_{\rm T1}}{\delta} T^{\omega+1/2} \frac{dT}{dr}, & r = R_1, \\ T_{\rm w2} - \frac{\xi_{\rm T2}}{\delta} T^{\omega+1/2} \frac{dT}{dr}, & r = R_2. \end{cases} \tag{10}$$

In these expressions, $\xi_{\rm T1}$ and $\xi_{\rm T2}$ are the temperature jump coefficients on the inner and outer cylinder surfaces, respectively. The assumption of a constant pressure between the cylinders is used to obtain the previous expressions. It is to note that the dimensionless value of the outer cylinder temperature is equal to 1, but in the following, the notation $T_{\rm w2}$ is retained for the convenience of presentation.

Using the dimensionless variables (9) and under the hypothesis of a constant pressure between the cylinders, Eq. (3) may be written as

$$\frac{\partial}{\partial r} \left(\mu r \frac{\partial T}{\partial r} \right) = 0. \tag{11}$$

Using the expression for heat flux (4), we obtain the energy conservation equation in the dimensionless form as

$$\frac{\partial(rq)}{\partial r} = 0, \qquad \text{where} \qquad q(r) = -\frac{15}{8\delta}\mu\frac{dT}{dr}. \tag{12}$$

The solution of Eq. (12) subjected to the temperature jump boundary condition (10) in the case of two known surface temperatures can be found in Ref. [12]. In order to write the completely explicit expression of the temperature distribution between the cylinders, a linearization of the temperature is carried out and the terms of the order of ε^2 are neglected, where $\varepsilon = (T_{\rm w} - T_{\rm g})/T_{\rm w}$, Eq. (7). If the heat flux on the inner cylinder is fixed, Eq. (12) can be solved to obtain the temperature profile between the cylinders with the accuracy ε^2 as

$$T(r) = \left(T_{\rm g2}^{\omega+1} + \frac{8\delta}{15}q_1 R_1\,(\omega+1)\ln\frac{R_2}{r}\right)^{\frac{1}{\omega+1}}, \tag{13}$$

with

$$T_{\rm g2}^{\omega+1} = T_{\rm w2}^{\omega+1}\left(1-(\omega+1)\mathcal{B}_2\right), \qquad \mathcal{B}_2 = -\frac{\xi_{\rm T2}}{\delta}\frac{\mathcal{A}}{R_2\sqrt{T_{\rm w2}}}, \tag{14}$$

and

$$\mathcal{A} = \frac{8}{15}\delta R_1 q_1. \tag{15}$$

The radial heat flux profile between the cylinders can be calculated as

$$q(r) = q_1\frac{R_1}{r} \tag{16}$$

and it deceases with the increase of r.

As it was mentioned above, in the slip flow regime the surface temperature can be different from the gas temperature near the surface. To find the internal surface temperature, $T_{\rm w1}$, the following equation has to be solved by the Newton method

$$\mathcal{A} = \frac{(T_{\rm w1}^{\omega+1} - T_{\rm w2}^{\omega+1})/(\omega+1)}{\ln(R_2/R_1) + \frac{\xi_{\rm T2}}{\delta R_2}T_{\rm w2}^{\omega+1/2} + \frac{\xi_{\rm T1}}{\delta R_1}T_{\rm w1}^{\omega+1/2}}, \tag{17}$$

where the value of $\mathcal{A}$ is calculated from Eq. (15).

4. Free Molecular Flow Regime

In the free molecular regime, the collisionless Boltzmann equation is solved to obtain the analytical expressions for number density, temperature, and heat flux. General formulation of all solutions can be written in dimensionless form as

- dimensionless number density

$$n(r) = \frac{n'(r)}{n_{av}} = \frac{1 - K_{\alpha 1} K_{T1} K_{R1}}{1 - K_{\alpha 1} K_{T1} K_{R2}}, \tag{18}$$

- dimensionless temperature

$$T(r) = \frac{T'(r)}{T_{w2}} = \frac{1 - K_{\alpha 1} K_{T2} K_{R1}}{1 - K_{\alpha 1} K_{T1} K_{R1}}, \tag{19}$$

- dimensionless heat flux

$$q(r) = \frac{q'(r)}{n_{av} k_B T_{w2} \sqrt{2 k_B T_{w2}/m}} = \frac{1}{\sqrt{\pi}} K_{\alpha 2} K_{T3} K_{R3} \frac{1}{1 - K_{\alpha 1} K_{T1} K_{R2}}, \tag{20}$$

where K_{α_i} and K_{T_i}, $i = 1, 2$, are the coefficients determined by the accommodation coefficients, α_1 and α_2 of each surface, and temperature of the hotter and colder surfaces,

$$\begin{aligned} &K_{\alpha 1} = \frac{\alpha_1 (2 - \alpha_2)}{\alpha_1 + \alpha_2 - \alpha_1 \alpha_2}, \qquad K_{\alpha 2} = \frac{\alpha_1 \alpha_2}{\alpha_1 + \alpha_2 - \alpha_1 \alpha_2}, \\ &K_{T1} = 1 - \sqrt{\frac{T_{w2}}{T_{w1}}}, \qquad K_{T2} = 1 - \sqrt{\frac{T_{w1}}{T_{w2}}}, \qquad K_{T3} = \frac{T_{w1}}{T_{w2}} - 1. \end{aligned} \tag{21}$$

The coefficients K_{R_i}, $i = 1, 3$, are determined by the geometry of the problem as

$$\begin{aligned} K_{R1} = \frac{1}{2} \frac{\arcsin(R_1/r)}{\pi/2}, \qquad K_{R2} = \frac{1}{2} \left\{ 1 - \frac{1}{\pi/2} \left[\frac{\arccos(\mathcal{R})}{1 - \mathcal{R}^2} - \frac{1}{\sqrt{\mathcal{R}^{-2} - 1}} \right] \right\}, \\ K_{R3} = \frac{R_1}{r}. \end{aligned} \tag{22}$$

The average number density is used in expressions (18) and (20) to normalize the number density. This averaged value is calculated as

$$n_{av} = \frac{2}{R_2^2 - R_1^2} \int_{R_1}^{R_2} n r dr. \tag{23}$$

For known cylinders' radii ratio, and fixed accommodation coefficients, the temperature of the inner cylinder surface can be found from the heat flux expression (20) calculated at the inner surface, $r = R_1$, by using the Cardano's formula to solve the depressed cubic equation [13].

5. Transitional Flow Regime

For the simulation of heat transfer in the transitional and near free molecular flow regimes, the S-model kinetic equation [4] is used. Considering the

axial symmetry of the problem, the S-model kinetic equation in the completely conservative form may be written as [14, 15, 16]

$$\frac{\partial}{\partial t'}\left(r'f'\right)+\frac{\partial}{\partial r'}\left(r'f'\upsilon_p\cos\varphi\right)-\frac{\partial}{\partial\varphi}\left(f'\upsilon_p\sin\varphi\right)=r'\nu'\left(f^{S'}-f'\right). \tag{24}$$

In this expression, $f'(t',r',\mathbf{v})$ is the one-particle molecular velocity distribution function, $\mathbf{v}=(\upsilon_p\cos\varphi,\upsilon_p\sin\varphi,\upsilon_z)$ is the molecular velocity vector with polar coordinates, υ_p and φ, which are the magnitude and orientation of velocity vector, respectively, and ν' is the molecular collision frequency. The ~~equilibrium~~ distribution function $f^{S'}$ in Eq. (24) has the form

$$f^{S'}=f^{M'}\left[1+\frac{2m\mathbf{v}\mathbf{q}'}{15n'\left(k_{\mathrm{B}}T'\right)^2}\left(\frac{m\mathbf{v}^2}{2k_{\mathrm{B}}T'}-\frac{5}{2}\right)\right] \tag{25}$$

with

$$f^{M'}(n',T')=n'\left(\frac{m}{2\pi k_{\mathrm{B}}T'}\right)^{3/2}\exp\left[-\frac{m\mathbf{v}^2}{2k_{\mathrm{B}}T'}\right], \tag{26}$$

where $f^{M'}$ is the local Maxwellian distribution function. The bulk velocity is equal to zero for this problem, and the heat flux vector has only one non-zero component along r-axis. In the frame of this model, the molecular collision frequency is supposed to be independent of the molecular velocities, and it is calculated as $\nu'=p'/\mu'$ [4]. The most probable molecular velocity υ_0, Eq. (1), is used to non-dimensionalize the molecular velocity $\mathbf{c}=\mathbf{v}/\upsilon_0$, where the dimensionless molecular velocity vector $\mathbf{c}$ is $(c_p\cos\varphi,c_p\sin\varphi,c_z)$. Using the dimensionless variables, Eq. (24) becomes

$$\frac{\partial(rf)}{\partial t}+\frac{\partial(rfc_p\cos\varphi)}{\partial r}-\frac{\partial(fc_p\sin\varphi)}{\partial\varphi}=r\delta nT^{1-\omega}(f^S-f). \tag{27}$$

Equation (27) is one-dimensional in the physical space, but three-dimensional in the molecular velocity space. The dependence of the distribution function on the c_z component of the molecular velocity vector is eliminated using the projection procedure, by introducing two reduced distribution functions [17]

$$\Phi(t,r,c_p,\varphi)=\int f(t,r,\mathbf{c})dc_z \quad\text{and}\quad \Psi(t,r,c_p,\varphi)=\int f(t,r,\mathbf{c})c_z^2dc_z. \tag{28}$$

After multiplying Eq. (27) by 1 and c_z^2, and integrating over c_z, the system of two kinetic equations is obtained as

$$\begin{aligned}\frac{\partial(r\Phi)}{\partial t}+\frac{\partial(r\Phi c_p\cos\varphi)}{\partial r}-\frac{\partial(\Phi c_p\sin\varphi)}{\partial\varphi}&=r\delta nT^{1-\omega}(\Phi^S-\Phi),\\ \frac{\partial(r\Psi)}{\partial t}+\frac{\partial(r\Psi c_p\cos\varphi)}{\partial r}-\frac{\partial(\Psi c_p\sin\varphi)}{\partial\varphi}&=r\delta nT^{1-\omega}(\Psi^S-\Psi).\end{aligned} \tag{29}$$

The relevant macroscopic flow parameters (number density, temperature and heat flux) are defined through the reduced distribution functions, respectively,

as

$$
\begin{aligned}
n(t,r) &= \iint \Phi(t,r,c_p,\varphi) c_p dc_p d\varphi, \\
T(t,r) &= \frac{2}{3n} \iint \left[c_p^2 \Phi(t,r,c_p,\varphi) + \Psi(t,r,c_p,\varphi)\right] c_p dc_p d\varphi, \\
q(t,r) &= \iint c_p \cos\varphi \left[c_p^2 \Phi(t,r,c_p,\varphi) + \Psi(t,r,c_p,\varphi)\right] c_p dc_p d\varphi \,.
\end{aligned} \tag{30}
$$

It is worth to note that the developed numerical approach allows us to obtain not only the steady state values of the macroscopic parameters, but also their evolution in time.

5.1. Boundary Conditions

In present simulations, the classical Maxwell diffuse-specular boundary conditions are used on both surfaces [6]. As gas between the two cylinders is considered at rest, so the accommodation coefficient in the diffuse-specular kernel is associated only to the thermal accommodation coefficient. Below, the classical constant temperature boundary condition at the outer wall and the new constant heat flux boundary condition at the inner wall are described.

5.1.1. Constant Surface Temperature

The temperature of the outer cylinder surface is maintained constant and equal to $T_{\mathrm{w}2}$, therefore the boundary condition for Eq. (27) at $r = R_2$ is

$$
f\left(t, R_2, c_p, \varphi\right) = \left(1-\alpha_2\right) f\left(t, R_2, c_p, \pi-\varphi\right) + \alpha_2 f^M\left(t, R_2, c_p, \varphi\right), \quad \frac{\pi}{2} \le \varphi \le \frac{3}{2}\pi, \tag{31}
$$

where α_2 is the accommodation coefficient at the outer cylinder surface. This boundary condition, (31), in terms of reduced distribution functions reads

$$
\begin{aligned}
&\Phi(R_2, c_p, \varphi) = (1-\alpha_2)\Phi(R_2, c_p, \pi-\varphi) + \alpha_2 \Phi^{\mathrm{M}}_{\mathrm{w}2}(R_2, c_p), \quad \text{for} \quad \frac{\pi}{2} \le \varphi \le \frac{3}{2}\pi, \\
&\text{with} \qquad \Phi^{\mathrm{M}}_{\mathrm{w}2}\left(R_2, c_p\right) = \frac{n_{\mathrm{w}2}}{\pi T_{\mathrm{w}2}} \, \exp\left(-\frac{c_p^2}{T_{\mathrm{w}2}}\right).
\end{aligned} \tag{32}
$$

The number density, $n_{\mathrm{w}2}$, is calculated from the no-penetration condition for the cylinder wall as

$$
n_{\mathrm{w}2} = -2\frac{\sqrt{\pi}}{\sqrt{T_{\mathrm{w}2}}} \int_0^{+\infty} c_p^2 dc_p \int_{\pi/2}^{3\pi/2} \Phi \cos\varphi d\varphi \,. \tag{33}
$$

5.1.2. Constant Heat Flux at the Surface

On the inner cylinder surface, constant heat flux, q_1, is applied. To derive the boundary condition for Eq. (27), corresponding to a fixed constant heat flux on the inner cylinder, we use two known relations. First of them, is the

impermeability (no-penetration) condition at the inner cylinder surface, *i.e.* the gas velocity normal to this surface is equal to zero

$$\int_{c_r<0} f c_r d\mathbf{c} + \int_{c_r>0} \left(\alpha_1 f^{\mathrm{M}} + (1-\alpha_1) f\right) c_r d\mathbf{c} = 0. \tag{34}$$

From previous relation, the unknown number density on the surface, $n_{\mathrm{w}1}$, can be expressed as a function of the incoming mass flux as

$$n_{\mathrm{w}1} = -\frac{2\sqrt{\pi}}{\sqrt{T_{\mathrm{w}1}}} \mathcal{M}_{\mathrm{in}}, \tag{35}$$

where the incoming mass flux, $\mathcal{M}_{\mathrm{in}}$, can be calculated as

$$\mathcal{M}_{\mathrm{in}} = \int_{c_r<0} f c_r d\mathbf{c}, \tag{36}$$

or using the reduced distribution function defined by Eq. (28)

$$\mathcal{M}_{\mathrm{in}} = \int_{-\pi/2}^{\pi/2} \Phi c_p^2 \cos\varphi dc_p d\varphi. \tag{37}$$

It is to underline that expressions (35) and (37) are independent of the accommodation coefficient on the inner surface, α_1, and that the surface temperature, $T_{\mathrm{w}1}$, in Eq. (35), is *a priori* unknown.

Then, we can write the analogous to Eq. (34) expression for the known heat flux on the inner cylinder surface, q_1, in term of incoming and outgoing fluxes as

$$q_1 = \int_{c_r<0} f c^2 c_r d\mathbf{c} + \int_{c_r>0} \left(\alpha_1 f^{M} + (1-\alpha_1) f\right) c^2 c_r d\mathbf{c}. \tag{38}$$

By simplifying the previous equation, we obtain the explicit expression for the heat flux as a function of incoming heat flux as

$$q_1 = \mathcal{H}_{\mathrm{in}} + \alpha_1 \frac{n_{\mathrm{w}1}}{\sqrt{\pi}} T_{\mathrm{w}1}^{3/2}, \tag{39}$$

where the incoming heat flux reads

$$\mathcal{H}_{\mathrm{in}} = \alpha_1 \int_{c_r<0} f c^2 c_r d\mathbf{c}. \tag{40}$$

By using the reduced distribution functions from Eqs. (28), expression (40) becomes

$$\mathcal{H}_{\mathrm{in}} = \alpha_1 \int_{c_r<0} c_p^2 \cos\varphi \left(c_p^2 \Phi + \Psi\right) dc_p d\varphi. \tag{41}$$

Putting together Eqs. (35), (37), (39), and (41), we finally obtain the system of two equations for unknown gas number density near the inner cylinder surface,

n_{w1}, and the surface temperature, T_{w1}, as a function of incoming mass and heat fluxes

$$T_{\mathrm{w1}} = \frac{\mathcal{H}_{\mathrm{in}} - q_1/\alpha_1}{2\mathcal{M}_{\mathrm{in}}}, \qquad \text{and} \qquad n_{\mathrm{w1}} = \frac{2\sqrt{\pi}}{\sqrt{T_{\mathrm{w1}}}}\mathcal{M}_{\mathrm{in}}. \tag{42}$$

The derivation of the constant heat flux boundary condition are provided here for the inner cylinder surface. However, this methodology can be applied to the outer cylinder or to other types of geometries.

5.2. Method of Solution

The applied numerical approach is analogous to that previously developed in Ref. [16]. First, the discrete velocity method (DVM) is used to separate the continuum molecular velocity space c_p in the system of kinetic equations (29) into discrete velocity set c_{p_k}. Next, the system of kinetic equations with discrete velocity set c_{p_k} is discretized in time and space by Finite Difference Method (FDM). The spatial derivatives are approximated by the first order-of-accuracy upwind-type numerical scheme. For the approximation of the time derivative, the explicit Euler scheme is used. The Gauss-Hermite quadrature formulas are chosen in order to evaluate the integrals for calculating the macroscopic parameters (30). These quadrature formulas insures for the low Mach number flows, which is the case of our study, the higher accuracy of integration with the smaller number of integration points compared with the Simpson rule, see for example Ref. [18].

In the physical space, the reduced distribution functions depend only on one variable r, which is the distance from the common axis of the two concentric cylinders. The distance between the cylinders is divided into N_r intervals. In the velocity space, the distribution functions depend on two variables; the magnitude and orientation of the molecular velocity vector, c_{p_k} and φ, respectively. The velocity vector magnitude c_{p_k} is distributed according to the Gaussian quadrature rule, which is characterized by the Gaussian abscissas N_{c_p} and their corresponding weights. The number of implemented N_{c_p} points depends on the gas rarefaction. The range of molecular velocity orientation ($0 \leq \varphi \leq \pi$) is divided into N_φ equal intervals. Moreover, this range of φ is divided into two subdomains, according to the sign of the molecular velocity components.

The time-explicit Euler method is based on the classical time derivation in a given point and on the space derivatives taken at the previous time step. Let us denote the numerical solution of the first partial derivative equation in (29) as $\Phi^l_{i,k,m} = \Phi(t^l, r_i, c_{p_k}, \varphi_m)$ and define $\Delta t^l = t^{l+1} - t^l$, where l denotes time level, $\Delta r = r_i - r_{i-1}$, and $\Delta\varphi = \varphi_m - \varphi_{m-1}$. For the case of $\cos\varphi_m > 0$ and

$\sin\varphi_m < 0$, the first equation of the system (29) can be approximated by

$$\frac{r_i\Phi^{l+1}_{i,k,m} - r_i\Phi^{l}_{i,k,m}}{\Delta t_l} + c_{p_k}\cos\varphi_m \frac{r_i\Phi^{l}_{i,k,m} - r_{i-1}\Phi^{l}_{i-1,k,m}}{\Delta r} - \\ -c_{p_k}\frac{\Phi^{l}_{i,k,m}\sin\varphi_{m+1/2} - \Phi^{l}_{i,k,m-1}\sin\varphi_{m-1/2}}{2\sin\frac{\Delta\varphi}{2}} = \\ = r_i\delta n^l_i \left(T_i^{1-\omega}\right)^l \left(\left(\Phi^S_{i,k,m}\right)^l - \Phi^l_{i,k,m}\right). \tag{43}$$

In the above approximation, the trigonometric correction [19] for the derivative of axisymmetric transport term (with respect to φ) is used. This scheme offers numerous properties [19] such as, uniform flow and positivity of the reduced distribution function preservations, and satisfaction of the conservation laws of the moments, and entropy dissipation.

For the temporal discretization, the time-step has to satisfy the classical Courant-Friedrichs-Lewy (CFL) condition [20] and must be smaller than the mean collision time, or relaxation time, which is inverse of the collision frequency ν. Hence, the time step must satisfy the following criterion

$$\Delta t \leq \mathrm{CFL}/\max_{i,k,m}\left(\frac{c_{p_k}}{\Delta r_i} + \frac{c_{p_k}}{r_0\Delta\varphi_m}, \nu_i\right) \tag{44}$$

with $\mathrm{CFL} = 0.95$. The calculations stop when the convergence criterion, defined as

$$||q_r||_{L_2} = \sqrt{\sum_{i=0}^{Nr}(q^{l+1}_{r_i} - q^l_{r_i})^2}/\sqrt{\sum_{i=0}^{Nr}(q^{l+1}_{r_i})^2} \tag{45}$$

and calculated using the L_2 norm, becomes smaller than $\varepsilon = 10^{-8}$.

6. Results and Discussion

In this Section, first, a parametrical study is conducted to quantify the influence of the inner and outer surface accommodation coefficients on the temperature difference between the two surfaces. Then, the proposed methodology is applied to simulate the temperature distribution between two concentric cylinders of real experimental conditions from Ref. [21].

6.1. Parametric Study

In this section, the effect of the thermal accommodation coefficients at both cylinders surfaces on the temperature difference, $\Delta T = T_{\mathrm{w1}} - T_{\mathrm{w2}}$ is analyzed. For this study, the heat flux on the inner cylinder is fixed to a constant value. However, due to the relation between dimensional and dimensionless values of the heat flux, Eq. (9), only the product $q_1\delta$ is constant when the rarefaction parameter changes. Therefore, depending on the value of rarefaction parameter, the heat flux is equal to $q_1 = 0.3, 0.03, 0.003$, and 0.0003 for the rarefaction

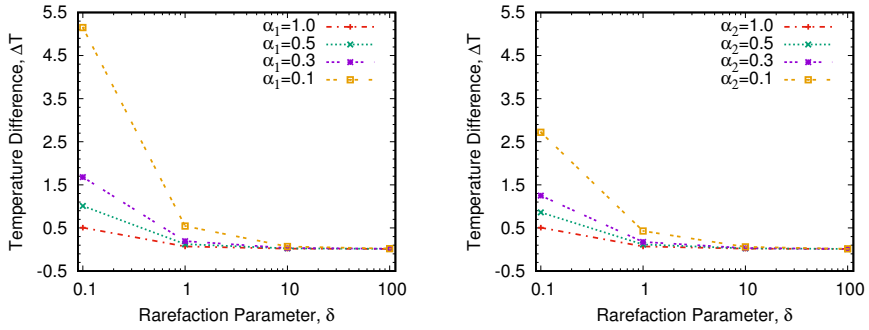

Figure 2: Dimensionless temperature difference between the inner and outer cylinder surfaces, $\Delta T = T_{w1} - T_{w2}$ as a function of the rarefaction parameter. (a) The accommodation coefficient on the outer cylinder surface, α_2, is fixed to 1 (diffuse reflection), while its value on the inner surface, α_1 is varied from 0.1 to 1. (b) The accommodation coefficient on the inner surface, α_1, is fixed to 1 (diffuse reflection), while its value on the outer surface, α_2 is varied from 0.1 to 1.

parameter equal to 0.1, 1, 10, and 100, respectively, with $q_1\delta = 0.03$. In these simulations the cylinders radii ratio, $\mathcal{R}$, is taken to be equal to 1.1.

For a fixed value of the heat flux at the inner cylinder surface and a fixed accommodation coefficient on both surfaces, the temperature difference, ΔT, increases with the decrease in the rarefaction parameter (see Fig. 2(a) and (b)). A pronounced increase of the temperature difference is observed when the rarefaction parameter decreases from 1 to 0.1. Comparing the two figures, one can observe that for a low rarefaction parameter ($\delta \leq 1$), the temperature difference is more affected by the decrease in the value of accommodation coefficient on the inner cylinder surface, α_1, than on the outer surface, α_2. This because the inner cylinder surface is hotter than the outer one, therefore, large temperature jumps are obtained on the inner wall when the accommodation coefficient is decreased. For $\delta > 10$, there is no significant effect on the temperature difference between the cylinders regardless of the thermal accommodation coefficient due to small effect of rarefaction.

It is well known [22] that at low pressure (high-rarefaction level) conditions, the surface temperature may be different from the gas temperature. The dimensionless temperature profiles are presented in Fig. 3 for three values of rarefaction parameter δ=0.1, 1 and 10, and for $\mathcal{R}$ =1.1 as a function of normalized distance between the cylinders. As in the previous case, the heat flux on the inner cylinder surface is fixed to be equal to $q_1\delta = 0.03$. In these simulations, the accommodation coefficient on both surfaces is set equal to 1. Figure 3 shows that the temperature in the gap increases as the gas becomes more rarefied (δ decreases). From the numerical simulations, the temperature of the inner surface is obtained to be equal to 1.507, 1.071 and 1.021 for δ=0.1, 1 and 10, respectively. The corresponding gas temperatures near the inner cylinder

surface are equal to 1.252, 1.049 and 1.019, respectively. As expected, larger temperature jumps and higher surface temperatures are obtained for higher rarefaction level, even if the same heat flux on the surface is maintained. It is to note that similar, but smaller in their amplitude, temperature jumps are observed on the outer cylinder surface, where the dimensionless temperature is fixed equal to 1.

This quantitative analysis is worth to be considered in practical applications. Very often, constant heat flux is applied to a surface to manage its temperature and a constant surface temperature is usually expected. However, if the gas pressure decreases considerably, for example by ten times, *i.e.* δ changes from 1 to 0.1, the surface temperature could increases by more than 40%.

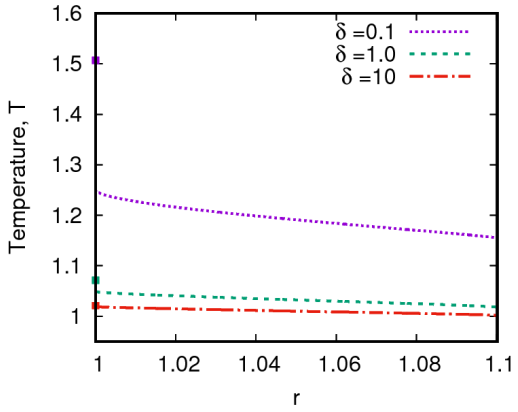

Figure 3: Dimensionless temperature in the gap between two cylinders, $\mathcal{R}$=1.1. The constant heat flux, q_1, equal to 0.003, 0.03 and 0.3 for δ equal to 10, 1, 0.1 respectively is fixed on the inner cylinder surface. The accommodation coefficients on both surfaces are assumed to be equal to 1. Points represents respective inner wall temperature T_{w1}.

In the continuum and slip flow regimes, the analytical expressions for the temperature and heat flux distributions are derived in Ref. [12] as a function of the surface temperatures. In the case, when the heat flux on the inner surface is known instead of the surface temperature, the temperature distribution in the gap can be calculated from Eq. (13). Figure 4(a) shows the temperature distribution between the cylinders for different values of the rarefaction parameter, ranging from near continuum ($\delta = 100$) to early transitional ($\delta = 1$) flow regimes. The temperature profiles are obtained from the numerical solution of the kinetic equation (solid lines) and from the analytical solution, Eq. (13) (dashed lines). As expected, a good agreement is found between the two approaches in the continuum and slip flow regimes, $\delta = 10$ and 100. The heat flux profiles in the gap are presented in Fig. 4(b). The profiles are obtained from the numerical solutions of the kinetic equation (solid lines) and analytical expression (16) (dashed lines). The heat flux profile in the gap is nearly constant for all considered values of gas rarefaction. A good agreement is found between

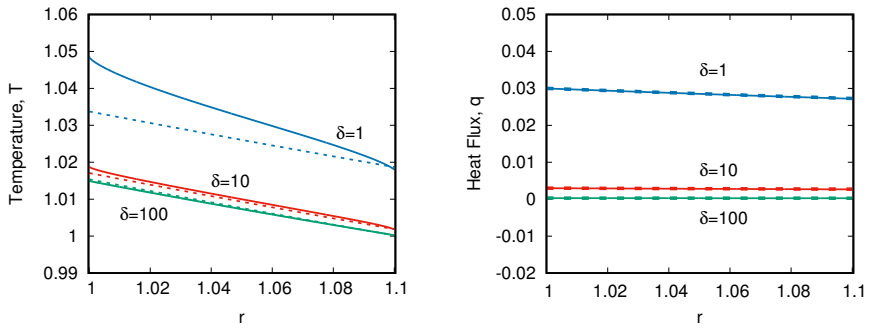

(a) (b)

Figure 4: Dimensionless temperature (a) and heat flux (b) in the gap between two cylinders, $\mathcal{R}$=1.1. The constant heat flux, q_1, equal to 0.0003, 0.003 and 0.03 for δ varies from 100 to 1, is fixed on the inner cylinder surface. The accommodation coefficients on both surfaces are assumed to be equal to 1. The results of kinetic simulations (solid lines) are compared with the analytical solutions (dashed line).

both approaches for δ=10 and 100.

In the free molecular regime, the analytical expressions for the temperature and heat flux distributions are also derived as a function of two known surface temperatures. In the case when the heat flux on one of the surfaces is known instead of surface temperature, the unknown surface temperature can be calculated from Eq. (20). Figures 5(a) and 5(b), respectively, show the temperature and the heat flux distributions in the gap for $\delta = 0.1$ and 0.01, which corresponds to the beginning and developed free molecular flow regime. The temperature and heat flux profiles are obtained from the numerical solution of the kinetic equation (solid lines), and from the analytical solution (dashed lines). To obtain the analytical solution, first, the inner surface temperature is obtained from Eq. (20) using information on the inner heat flux, q_1, then the temperature and heat flux profiles are obtained using Eqs. (19) and (20). A very good agreement is obtained for both profiles at both rarefaction levels.

6.2. Comparison with Experimental Results

Kinetic numerical simulations of the temperature distribution are conducted for a configuration similar to the experimental setup presented in Ref. [21]. The experimental results are used to validate the proposed formulation of constant heat flux boundary condition for the kinetic equation. The experimental setup consists of two concentric stainless steel cylinders spaced by a gap, $R_0 = R'_2 - R'_1$=2mm with R'_1= 43.5mm. The inner cylinder consists of a cartridge heater centered inside a thick aluminum cylinder, which is surrounded by a thin stainless steel sheath. The outer cylinder consists of a stainless steel pressure vessel surrounded by a water jacket to control its temperature. The length of the inner cylinder is 1.031m, and the length of the outer vessel cylinder is 1.422m. Therefore, the inner cylinder is fully contained inside the outer

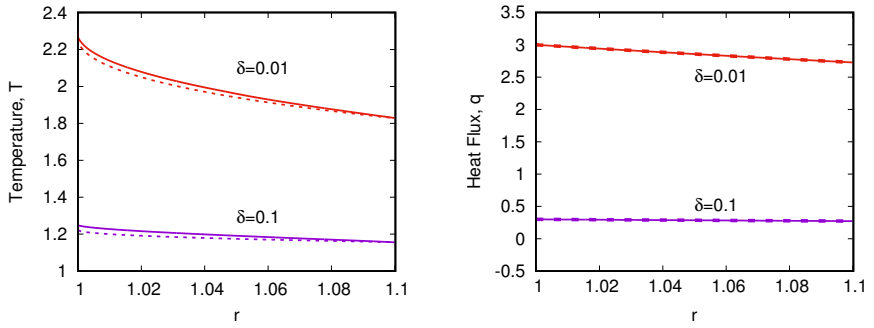

(a) (b)

Figure 5: Dimensionless temperature (a) and heat flux (b) in the gap between two cylinders, $\mathcal{R}$=1.1. The constant heat flux, q_1, equal to 0.3 and 3 for δ=0.1 and 0.01, respectively. The accommodation coefficients on both surfaces are assumed to be equal to 1. The results of kinetic simulations (solid lines) are compared with the analytical solutions (dashed line).

cylinder. Supports attached to both ends of the inner cylinder maintain concentricity between the inner and outer cylinders. The supports were designed to have small contact areas to prevent heat loss through conduction at the two ends of the inner cylinder. To measure the temperature of the inner cylinder, twelve thermocouples are placed between the aluminum cylinder and the stainless steel sheath in small grooves at three different axial locations. Other twelve thermocouples are placed on the outer surface of the outer cylinder at the same axial locations as the inner thermocouples to measure the temperature of the outer cylinder.

For all experiments, the temperature of the outer cylinder surface is maintained constant at $T_{w2} = 295 \pm 1$ K. For each experiment, the gap is initially filled with helium at the desired initial pressure, then the cartridge heater is tuned on to generate heat at the desired value. The experiment is conducted until both temperature and pressure reach steady-state. The temperatures and pressure are then collected and averaged over few hours past steady-state. Different total heat generation rates, Q_T, varying from 100W to 500W, are applied to the inner cylinder. As mentioned before, the experiment was designed to minimize heat losses from the ends of the inner cylinder and to ensure that most of the generated heat leaves through the annular gap between the cylinders. However, even with this design, there was still some heat losses through the ends of the inner cylinder, either by conduction or radiation, referred to by Q_L. This end heat loss is estimated in the continuum regime by comparing the experimental data to the one-dimensional analytical solution of heat transfer between concentric cylinders. Also, a portion of the heat though the gap is transfered by radiation, which is referred to by Q_R. The amount of heat transferred by conduction, Q_C, is calculated as $Q_C = Q_T - Q_R - Q_L$, see Table 1. The total heat generation, Q_T, and the portion transferred by conduction, Q_C, through

the gap, as well as the measured initial, $p_{\rm ini}$, and steady state, $p_{\rm ss}$, pressures in the gap, and the inner cylinder surface temperature, $T_{\rm w1}^{\rm exp}$, are provided in Table 1. The accommodation coefficients on both surfaces are estimated in Ref. [21] to be the same and their values are also presented in Table 1.

The temperature distribution in the gap between the cylinders was simulated using the numerical solution of the S-model kinetic equation for different values of heat flux imposed on the inner cylinder surface. The cylinders length is large compared to their radii, so the experimental configuration is simulated as one dimensional, considering only the cylinders cross-section. The value of the heat flux q_1 at the inner cylinder surface is calculated from the portion of heat transferred by conduction, Q_C, by dividing it by the inner cylinder surface area. The outer cylinder surface temperature is fixed to be equal to the measured value. The initial pressure measured in the gap is used to calculate the rarefaction parameter δ.

The values of the simulated temperature of the inner cylinder surface, $T_{\rm w1}^{\rm sim}$, are shown in Table 1 and are compared with the experimental values. For each experimental condition, the relative error between the measured and simulated inner temperatures are also provided in Table 1. This table shows that there is a good agreement between both temperatures with a maximum error on the order of 2.8% obtained for case 10. However, for all the other cases, the error is less than 1

In Section 3, the analytical expressions of temperature and heat flux distributions, Eqs. (13) and (16), in the gap are provided, which are valid in the slip and continuum flow regimes. The values for the inner cylinder temperature, $T_{\rm w1}^{\rm an}$, calculated from Eqs. (17) and (15) using Newton method, are provided in Table 1. A very good agreement is found with the measured values for all cases with an error less than 1.4%. The maximum deviation is obtained for case 10.

N	$Q_T[W]$	Q_C [W]	$p_{\rm ini}$ [Pa]	$p_{\rm ss}$[Pa]	α	$T_{\rm w1}^{\rm exp}$ [K]	$T_{\rm w1}^{\rm sim}$ [K]	% error	$T_{\rm w1}^{\rm an}$ [K]
1	100	92.0	104.5	108.4	0.374	314.6	315.2	0.19	313.6
2	100	92.3	139.6	140.5	0.364	312.1	312.3	0.08	310.9
3	200	183.8	101.0	107.9	0.375	335.5	337.2	0.51	334.9
4	200	184.4	141.9	146.1	0.360	330.1	330.8	0.21	328.5
5	300	275.2	107.2	121.3	0.366	356.4	355.9	0.13	353.7
6	300	276.0	134.6	153.2	0.389	346.6	346.6	0.00	344.0
7	400	366.7	109.1	119.7	0.353	375.2	375.6	0.11	374.3
8	400	367.8	140.6	152.3	0.354	363.5	365.9	0.66	363.6
9	500	457.1	107.3	110.3	0.363	395.4	393.8	0.40	393.8
10	500	458.4	138.5	139.6	0.369	383.7	372.9	2.82	378.4

Table 1: Comparison between experimental [21], numerical and analytical data for different total heat generation rates, Q_T and pressures in the gap.

Fig. 6 shows the temperature difference between the inner and outer cylinders obtained from the experiments, analytical solution, and numerical simulations as a function of the inverse of pressure. Good agreement was found between experimental, numerical and analytical results. The slight deviation of analytical and numerical results from the measured data for case 10 can be

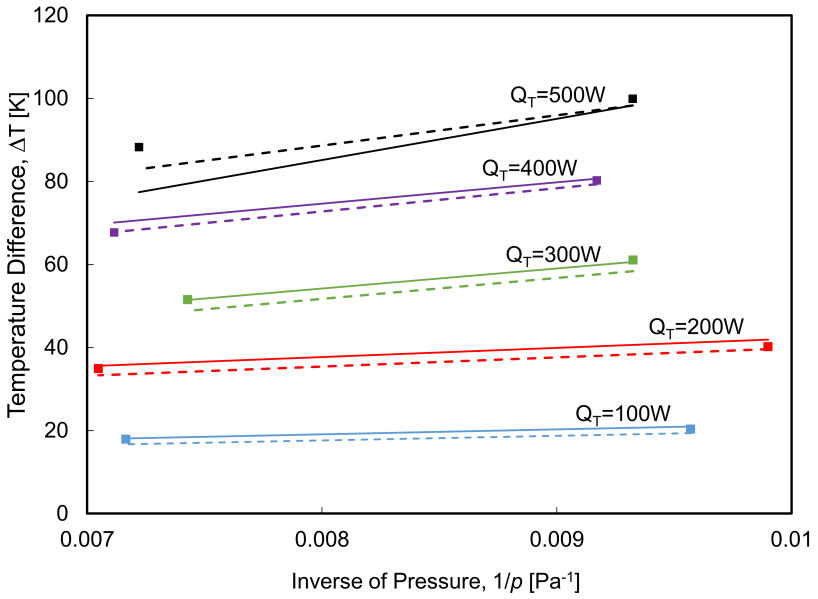

Figure 6: Measured, simulated and analytical values of temperature difference between the inner and outer cylinders as a function of the inverse of pressure for all heat generation rates. Solid line represent numerical results obtained by proposed simulation technique, dashed line show results obtained through analytical expression, (13), experimental results [21] are represented by the symbols.

attributed to inaccuracy of the methodology used in Ref. [21] to calculate the thermal accommodation coefficient, which is based on the implementation of the analytical formulation available in the slip flow regime [23].

As it was mentioned in Section 5, the developed approach allows the simulation of the transient behavior of temperature in the gap. The time evolution of the inner surface temperature T_{w1} obtained from the experimental data and the numerical simulations are compared in Fig. 7 for case 9 (see Table 1). The "numerical" time was rescaled to match with the experimental one, because the temperature evolution was simulated only in a slice of the experimental configuration, instead of the full length of the cylinders. This figure shows that the simulated temperature of the inner cylinders closely follow the experimental data. The same result was obtained for the other cases.

7. Conclusion

In this work, a new constant heat flux boundary condition is developed in the frame of the kinetic approach, which is valid in all gas rarefaction range. In addition, the analytical expression of the temperature and heat flux in the gap are derived in the slip flow regime by using the temperature jump conditions. The surface temperature, which is different from the gas temperature can be also obtained using the Newton method.

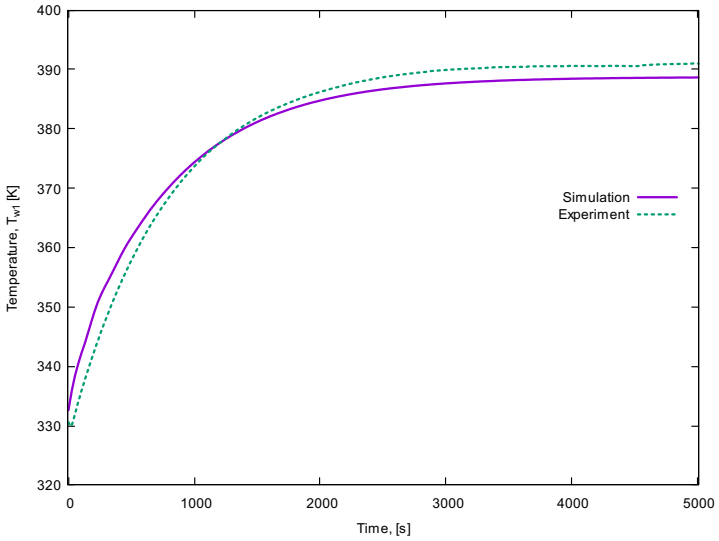

Figure 7: Comparison of time evolution of inner wall temperature T_{w1} for both experimental and simulation results.

Under the free molecular flow conditions the expression for the temperature and heat flux are obtained for the arbitrary values of the accommodation coefficients. The surface temperature under constant heat flux boundary condition is calculated from the depressed cubic equation for free molecular flow condition.

Both, analytical and numerical approaches are compared to determine the validity ranges for the analytical expression. Then, the numerical simulations are compared to experimental data of heat transfer between two concentric cylinders. A very good agreement was found between the numerical, analytical, and experimental results in the considered range. The proposed analytical relations could be useful for many engineering applications.

Acknowledgments

The work of the authors, Mustafa Hadj-Nacer, Cody Zampella, and Miles Greiner, was supported by the U.S. Department of Energy Office of Nuclear Energy University Program under award number DE-NE0008713, and the Nuclear Regulatory Commission under award number NRC-HQ-13-G-38-0027.

[1] Q. W. Wang, C. L. Zhao, M. Zheng, and N. Y. E. Wu, Numerical Heat Transfer Part B **53**, 150 (2008).

[2] H. Akhlaghi, E. Roohi, and S. Stefanov, Int. J. Therm. Sci. **59**, 111 (2012).

[3] J. Meng, Y. Zhang, and R. J. M, Commun. Comput. Phys. **17**, 1185 (2015).

[4] E. M. Shakhov, Fluid Dyn. **3**, 95 (1968).

[5] G. A. Bird, Molecular Gas Dynamics and the Direct Simulation of Gas Flows (Oxford Science Publications, Oxford University Press Inc., New York, 1994).

[6] C. Cercignani, Mathematical methods in kinetic theory (Premuim Press, New York, London, 1990).

[7] M. N. Kogan, Rarefied gas dynamics (Plenum Press New York, 1969).

[8] J. T. Lin and D. R. Willis, Phys. Fluids **15**, 31 (1972).

[9] T. F. Morse, Physics of Fluids (1964).

[10] L. H. Holway, Physics of fluids **9**, 1658 (1966).

[11] P. Welander, Ark. Fys. **7**, 507 (1954).

[12] I. Graur, M. T. Ho, and M. Wuest, Journal of Vacuum Science & Technology A: Vacuum, Surfaces, and Films **31**, 061603 (2013).

[13] M. Hazewinkel, Encyclopedia of Mathematics, Cardano formula, 2nd ed. (Springer Science+Business Media B.V./Kluwer Academic Publishers, 2001).

[14] I. N. Larina and V. A. Rykov, Comput. Math. Math. Phys. **38**, 1335 (1998).

[15] E. M. Shakhov and V. A. Titarev, European Journal of Mechanics B/Fluids **28**, 152 (2009).

[16] M. T. Ho and I. Graur, Vacuum **109**, 253 (2014).

[17] H. Yamaguchi, K. Kanazawa, Y. Matsuda, T. Niimi, A. Polikarpov, and I. Graur, Physics of Fluids **24** (2012).

[18] A. N. Kudryavtsev and A. A. Shershnev, J Sci Comput **57**, 42 (2013).

[19] L. Mieussens, J. Comput. Phys. **162**, 429 (2000).

[20] R. Courant, K. Friedrichs, and H. Lewy, IBM Journal on Research and development **11**, 215 (1967).

[21] C. Zampella, M. Lane, M. Hadj Nacer, and M. Greiner, in Proceedings of the 19th International Symposium on the Packaging and Transportation of Radioactive M (PATRAM, 2019) pp. 1–10.

[22] C. Cercignani, Theory and application of the Boltzmann equation (Scottish Academic Press, Edinburgh, 1975).

[23] H. Yamaguchi, T. Imai, T. Iwai, A. Kondo, Y. Matsuda, and T. Niimi, Journal of Vac. Sci. Technol. A **32**, 061602 (2014).